Clumped isotope evidence for Early Jurassic extreme polar warmth and high climate sensitivity

Thomas Letulle, Guillaume Suan, Mathieu Daëron, Mikhail Rogov, Christophe Lécuyer, Arnauld Vinçon-Laugier, Bruno Reynard, Gilles Montagnac, Oleg Lutikov, Jan Schlögl

Clim. Past, 18, 435–448, 2022
https://doi.org/10.5194/cp-18-435-2022

Climate of the Past
Open Access
EGU

Clumped isotope evidence for Early Jurassic extreme polar warmth and high climate sensitivity

Thomas Letulle[1], Guillaume Suan[1], Mathieu Daëron[2], Mikhail Rogov[3], Christophe Lécuyer[1], Arnauld Vinçon-Laugier[1], Bruno Reynard[1], Gilles Montagnac[1], Oleg Lutikov[3], and Jan Schlögl[4]

[1]Univ Lyon, UCBL, ENSL, UJM, CNRS, LGL-TPE, 69622, Villeurbanne, France
[2]Laboratoire des Sciences du Climat et de l'Environnement, LSCE/IPSL, CEA-CNRS-UVSQ, Université Paris-Saclay, Orme des Merisiers, 91191 Gif-sur-Yvette CEDEX, France
[3]Laboratory of Phanerozoic Stratigraphy, Geological Institute of Russian Academy of Sciences, 119017 Moscow, Russia
[4]Department of Geology and Palaeontology, Faculty of Natural Sciences, Comenius University, Mlynská dolina G, 842 15 Bratislava, Slovak Republik

Correspondence: Thomas Letulle (thomas.letulle@univ-lyon1.fr)

Received: 29 June 2021 – Discussion started: 29 July 2021
Revised: 21 January 2022 – Accepted: 25 January 2022 – Published: 4 March 2022

Abstract. Periods of high atmospheric CO_2 levels during the Cretaceous–early Paleogene ($\sim$ 140 to 34 Myr ago) were marked by very high polar temperatures and reduced latitudinal gradients relative to the Holocene. These features represent a challenge for most climate models, implying either higher-than-predicted climate sensitivity to atmospheric CO_2 or systematic biases or misinterpretations in proxy data. Here, we present a reconstruction of marine temperatures at polar ($> 80°$) and middle ($\sim 40°$) paleolatitudes during the Early Jurassic ($\sim$ 180 Myr ago) based on the clumped isotope (Δ_{47}) and oxygen isotope ($\delta^{18}O_c$) analyses of shallow buried pristine mollusc shells. Reconstructed calcification temperatures range from ~ 8 to $\sim 18\,°C$ in the Toarcian Arctic and from ~ 24 to $\sim 28\,°C$ in Pliensbachian mid-paleolatitudes. These polar temperatures were $\sim$ 10–20 °C higher than present along with reduced latitudinal gradients. Reconstructed seawater oxygen isotope values ($\delta^{18}O_w$) of -1.5 ‰ to 0.5 ‰ VSMOW and of -5 ‰ to -2.5 ‰ VSMOW at middle and polar paleolatitudes, respectively, point to a significant freshwater contribution in Arctic regions. These data highlight the risk of assuming the same $\delta^{18}O_{sw}$ value for $\delta^{18}O$-derived temperature from different oceanic regions. These findings provide critical new constraints for model simulations of Jurassic temperatures and $\delta^{18}O_{sw}$ values and suggest that high climate sensitivity has been a hallmark of greenhouse climates for at least 180 Myr.

1 Introduction

Proxy data indicate that the Cretaceous–early Paleogene ($\sim$ 140 to 34 Myr ago) was characterized by high atmospheric CO_2 concentrations, extreme polar warmth, and reduced latitudinal temperature gradients (Sluijs et al., 2006; Suan et al., 2017; Evans et al., 2018). Most state-of-the-art climate models hardly reproduce such features, implying either a higher climate sensitivity under greenhouse conditions or systematic biases in proxy data interpretation (Huber and Caballero, 2011; Laugié et al., 2020; Zhu et al., 2020). It remains unclear whether higher climate sensitivity is unique to the Cretaceous–early Paleogene world or is rather a hallmark of Earth's climate under high atmospheric pCO_2. Temperature proxies sensitive to overwriting under important burial, such as molecular or clumped isotope thermometry (Henkes et al., 2014; Fernandez et al., 2021; Hemingway and Henkes, 2021), have seldom been applied to older sediments owing to their generally higher thermal maturity (Robinson et al., 2017; Ruebsam et al., 2020; Fernandez et al., 2021). Consequently, current temperature estimates predating the Cretaceous period are mostly derived from the oxygen isotope composition of marine carbonate fossils ($\delta^{18}O_c$), with well-known limitations related to uncertainties in the past $\delta^{18}O$ signature of seawater ($\delta^{18}O_w$) (Epstein et al., 1953; Roche et al., 2006; Laugié et al., 2020).

Here, we use carbonate clumped isotope thermometry (Δ_{47}) to simultaneously constrain the calcification temperatures and associated $\delta^{18}O_w$ values of marine carbonate shells (mostly aragonite) collected from Lower Jurassic sedimentary successions with exceptionally shallow to moderate burial depths spanning subtropical to polar paleolatitudes. We compare our results to existing Jurassic to Eocene climate proxy data and simulations and discuss their implications for climate sensitivity under greenhouse conditions.

2 Geological settings

2.1 Polovinnaya River

The Polovinnaya River section is located in northern Siberia (72°36′05″ N, 107°58′52.2″ E) and was located near the North Pole during the Early Jurassic (Fig. 1). Our bivalve samples come from between 0 and 14 m in the section and belong to the Toarcian (Suan et al., 2011). This interval consists of silty shale slightly enriched in organic carbon (TOC $\sim$ 0.5 %). Except for localized carbonate concretions, there is no carbonate fraction in the sediment. The studied interval has been previously correlated with the lower Toarcian serpentinum ammonite zone based on biostratigraphy of foraminifera as well as dinoflagellate cyst and lithostratigraphic correlation with other sections of the basin (Suan et al., 2011). This section records very abundant *Dacryomya* bivalve shells (Fig. S1 in the Supplement), an opportunistic suspension-feeder genus tolerant to poorly oxygenated waters, which preferred conditions with weak hydrodynamics (Zakharov and Shurygin, 1978). A few belemnite rostra were also recorded, as were isolated fish scales and teeth. Overall the fossil assemblage indicates fully marine conditions within proximity of the continents as evidenced by the occurrence of wood debris. The section has undergone low burial as suggested by the low values of Rock-Eval pyrolysis T_{max} (mean = 420 °C) previously measured in the host sediments (Suan et al., 2011). Regional stratigraphy from the more distal Anabar area suggests local overburden not exceeding 1000 m: a total overburden (lower Toarcian to Valanginian) of about 380 m is recorded in the Anabar River area (Nikitenko et al., 2013) located 200 km east of the Polovinnaya section, which may be extended to about 1000 m when adding Valanginian–Cenomanian overburden from the more distal Bol'shoi Begichev islands. Modern local geothermal fluxes are lower than 50 mW m^{-2} (Kerimov et al., 2020), indicative of a low geothermal gradient (< 25 °C km^{-1}). Assuming a warm mean surface temperature of 10 °C, 1000 m of overburden, and that the geothermal gradient of the Siberian craton did not significantly change in the last 200 Myr, maximum burial temperatures of around 35 °C can be estimated for the studied specimens from the Polovinnaya River.

2.2 Warcq

Samples from the north-eastern Paris Basin were collected in 2014 from a temporary road cutting located near Warcq, Ardennes, France (49°45′21.6″ N, 4°39′28.8″ E). They consist of grey silty claystone with lenses of packed carbonated shell fragments, mainly from a variety of bivalves (*Grammatodon*, *Malletia*, *Limea*, *Oxytoma*) and a few ammonoids (*Beaniceras*, *Aegoceras ?*, Dactylioceratidae) (Fig. 2). The lithology, fossil preservation, and assemblages of the sampled beds are similar to those described by Thuy et al. (2011) from a nearby site in Sedan dated from the Pliensbachian Davoei zone. The sampled levels are therefore tentatively attributed to the lower Pliensbachian Davoei ammonite zone. Mean T_{max} values of 425 °C and maximum burial temperatures near 60 °C have been reported for Pliensbachian sediments from NE Paris Basin boreholes where the Davoei zone is $\sim$ 1100 m deep in the EST 433 borehole, some 150 km south from Warcq (Blaise et al., 2014), and at $\sim$ 860 m in the Montcornet borehole, some 50 km west from Warcq (Disnar et al., 1996; Bougeault et al., 2017). These burial temperatures and depth should be regarded as an upper limit, as the very proximal sampling area near Warcq repeatedly emerged during the Mesozoic and hence shows a much thinner Mesozoic cover of $\sim$ 500 m compared to these more distal sites (Waterlot et al., 1960). Assuming 860 m of overburden, $\sim$ 300 m of Cretaceous overburden eroded during the Cenozoic based on Paris Basin thermal history (Brigaud et al., 2020), a Mesozoic surface temperature of $\sim$ 20 °C, and a canonical continental geothermal gradient of $\sim$ 35 °C km^{-1}, maximal burial temperature of $\sim$ 60 °C can be estimated for the studied specimens from Warcq.

3 Material and methods

3.1 Sampled material

The two studied sites present exceptionally rare records of aragonite preservation for the Lower Jurassic interval. *Dacryomya* shells are the most abundant macrofossil and the only bivalve genus to occur in the Polovinnaya River section. They are very abundant in the lower part of the section (0 to 8 m). They are mainly represented by adult shells, while juveniles are common in only a few levels. They appear as $\sim$ 1 cm distinct individual or detached valves, sometimes close to each other (Fig. 2). The carbonate shells, commonly flattened and partially to entirely preserved, are a few millimetres thick but brittle and detached easily from their inner and outer mould. Their cream to white colour contrasts with the dark aspect of the sediment, and a few thicker individuals are iridescent.

Mollusc shells from Warcq clearly show a more energetic environment as they mostly appear as packed shell fragments with higher taxonomic diversity relative to the other site. A few complete individuals and separated valves can be ob-

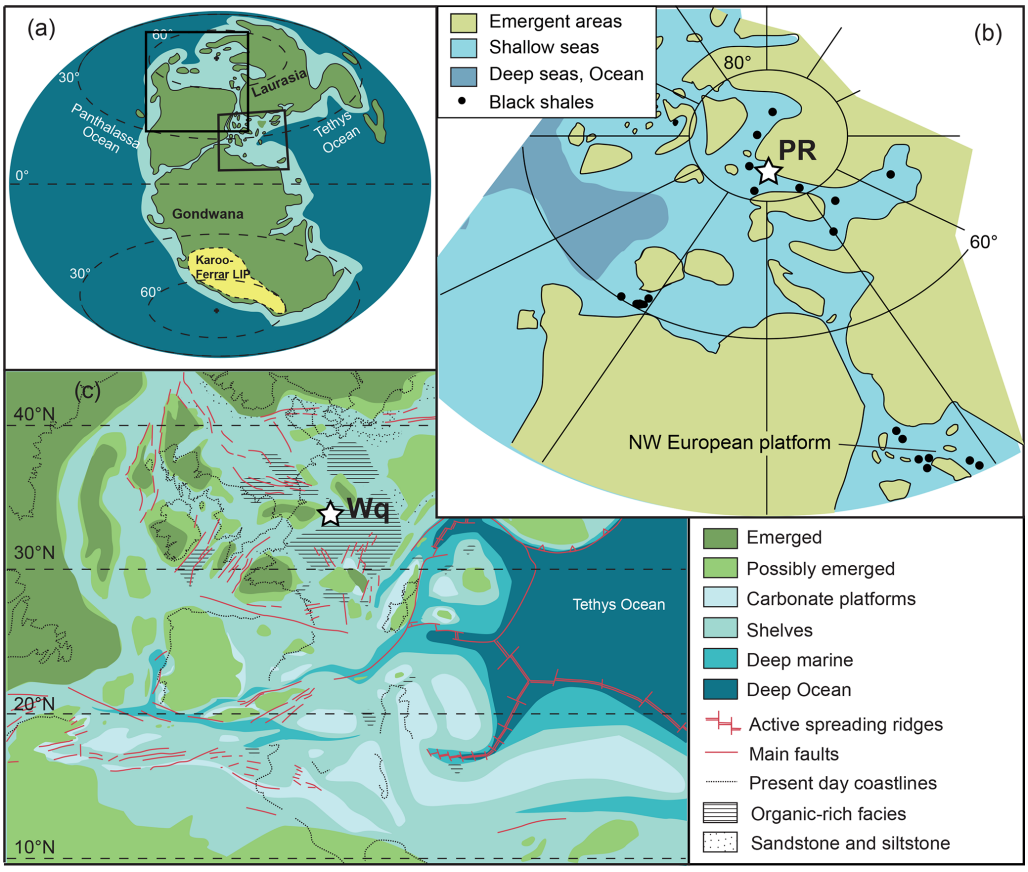

Figure 1. Location of the studied sites with regard to Toarcian (Early Jurassic) geography. **(a)** Global map modified from Dera et al. (2009). **(b)** Arctic map modified from Nikitenko and Mickey (2004). **(c)** Tethyan map modified from Thierry (2000). Localities: PR – Polovinnaya River; Wq – Warcq.

served among the debris with their associated mould in or around the remaining shell. Shells are cream to clear white, with some showing iridescence.

The remnants of carbonate shells were sampled as a whole using dental tools under a binocular microscope. A carbonate vein and matrix from the carbonate nodule POL-29 were also sampled to constrain the geochemistry of this potential diagenetic phase.

The microstructural preservation state and mineralogy of the analysed bivalve and ammonite shells were investigated using a Phenom Pure G2 scanning electron microscope (SEM) in backscatter mode and Raman spectroscopy using an XploRA Raman microscope in the Laboratoire de Géologie de Lyon (LGL-TPE). SEM observations were performed on relatively large fragments of the most complete specimens. Raman spectra were acquired either directly on the fossil specimens partly enclosed in the sedimentary matrix or on several grains of the sampled powders.

3.2 Geochemical analysis and data processing

The Δ_{47} and $\delta^{18}O$ values of 15 samples were measured (one to five replicates each) using methods described by Daëron et al. (2016). Carbonate samples were converted to CO_2 by phosphoric acid reaction at 90 °C in a common, stirred acid bath for 15 min. Initial phosphoric acid concentration was 103 % (1.91 g cm^{-3}), and each batch of acid was used for 7 d. After cryogenic removal of water, the evolved CO_2 was helium-flushed at 25 mL min^{-1} through a purification column packed with Porapak Q (50/80 mesh, 1 m length, 2.1 mm i.d.) and held at −20 °C, then quantitatively recollected by cryogenic trapping and transferred into an Isoprime 100 dual-inlet mass spectrometer equipped with six Faraday collectors (m/z 44–49). Each analysis took about 2.5 h, during which analyte gas and working reference gas were allowed to flow from matching 10 mL reservoirs into the source through deactivated fused silica capillaries (65 cm length, 110 µm i.d.). Every 20 min, gas pressures were adjusted to achieve $m/z = 44$ current of 80 nA, with differences between analyte gas and working gas generally below 0.1 nA. Pressure-dependent background current correc-

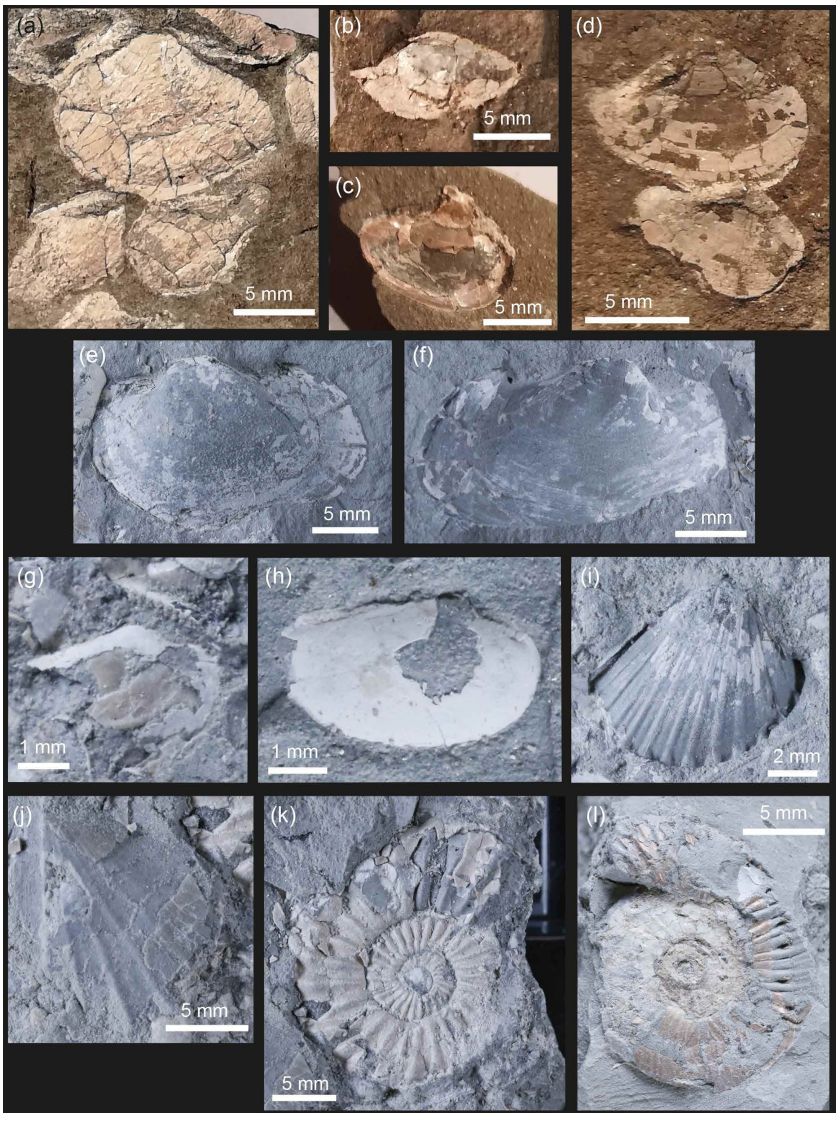

Figure 2. Selected specimens from the sampled successions. **(a–d)** Polovinnaya River section (Toarcian). **(e–l)** Warcq section (Pliensbachian). **(a)** *Dacryomya jacutica*, specimen POL-29 (on the surface of a carbonate concretion). **(b)** *Dacryomya jacutica*, specimen POL-13. **(c, d)** *Dacryomya jacutica*, specimen POL-05. **(e, f)** *Grammatodon* sp., specimen ARD-01 (inner **e** and outer **f** mould after sampling of the shell). **(g, h)** *Malletia* sp. **(i)** *Limea* sp., specimen ARD-03 (inner mould after sampling of the shell). **(j)** *Oxytoma* sp. ind. (inner mould with remains of a calcite shell). **(k)** *Aegoceras ?*, specimen ARD-06. **(l)** Dactylioceratidae indet., specimen ARD-07.

tions were measured 12 times for each analysis. All background measurements from a given session are then used to determine a mass-specific relationship linking background intensity (Zm), total $m/z = 44$ intensity ($I44$), and time (t): $\mathrm{Zm} = a + bI44 + ct + dt2$. Background-corrected ion current ratios ($\delta45$ to $\delta49$) were converted to $\delta^{13}C$, $\delta^{18}O$, and "raw" Δ_{47} values as described by Daëron et al. (2016) using the IUPAC oxygen-17 correction parameters. The isotopic composition ($\delta^{13}C$, $\delta^{18}O$) of our working reference gas was computed based on the nominal isotopic composition of carbonate standard ETH-3 (Bernasconi et al., 2018) and an oxygen-18 acid fractionation factor of 1.00813 (Kim et al., 2007). Raw Δ_{47} values were then converted to the Intercarb-Carbon Dioxide Equilibrium Scale (I-CDES) Δ_{47} reference frame by comparison with four "ETH" carbonate standards (Bernasconi et al., 2021) using a pooled regression approach (Daëron, 2021). Full analytical errors are derived from the external reproducibility of unknowns and standards ($\mathrm{Nf} = 89$) and conservatively account for the uncertainties in raw Δ_{47} measurements as well as those associated with the conversion to the "absolute" Δ_{47} reference frame.

Complementary $\delta^{13}C$ and $\delta^{18}O$ analyses of the smallest Arctic shells were performed at LGL-TPE using a Multiprep™ automated sampler coupled to a dual-inlet GV Iso-

prime™ mass spectrometer. Samples were reacted with anhydrous phosphoric acid at 90 °C. Duplicated samples were adjusted to the international references NIST NBS 18 and NBS 19 as well as in-house standard Carrara Marble. Since 2019 overall reproducibility of the in-house standard Carrara Marble has been ± 0.088 ‰ for $\delta^{18}O$ (2 SE, $n = 649$) and ± 0.064 ‰ for $\delta^{13}C$ (2 SE, $n = 649$) with mean $\delta^{18}O$ and $\delta^{13}C$ values of −1.041 ‰ and +2.025 ‰ (VPDB), respectively. All carbonate isotopic values ($\delta^{13}C$, $\delta^{18}O_c$) are reported in ‰ VPDB.

Clumped isotope temperatures were computed based on the I-CDES calibration of Anderson et al. (2021). Temperature uncertainties correspond to the fully propagated 95 % confidence intervals from Δ_{47} measurements of each sample (Daëron, 2021), neglecting the much smaller uncertainties in the calibration. The $\delta^{18}O$ values from aragonite samples were adjusted considering the different phosphoric acid fractionation factors for calcite and aragonite (Kim et al., 2007). The $\delta^{18}O_w$ values relative to VSMOW were estimated using Δ_{47}-derived temperatures and the equations of Grossman and Ku (1986) and Kim and O'Neil (1997) for mollusc shells and calcite vein, respectively.

Paleolatitude of the studied sites was computed using the online paleolatitude calculator paleolatitude.org (van Hinsbergen et al., 2015) computed with the model of Torsvik et al. (2012).

4 Results

4.1 Polovinnaya River, Siberia

The SEM observations of shell fragments of *Dacryomya jacutica* revealed well-preserved sheet nacreous microstructures underlying a prismatic layer we interpret as the outer shell layer (Fig. 3). All Raman spectra gathered from *Dacryomya jacutica* shells confirm that the original aragonite mineralogy is preserved.

The Δ_{47} values range from 0.6151 ± 0.0108 ‰ to 0.6457 ± 0.0182 ‰ I-CDES for Siberian aragonite bivalves, with a Δ_{47} of 0.5752 ± 0.0134 for the fracture-infilling calcite vein. Reconstructed Δ_{47} temperatures, applying the equation of Anderson et al. (2021), range from 8.8 ± 5.2 to 18.0 ± 3.4 °C for Siberian bivalves and 31.5 ± 4.8 °C for the calcite vein.

Mean $\delta^{18}O_c$ values are −2.73 ± 0.71 ‰ (1 SD, $n = 31$, max = 0.36, min = −5.08 ‰) for Siberian bivalves and −14.21 ± 0.02 ‰ for the fracture-infilling calcite vein, while the carbon isotope values ($\delta^{13}C$) range from 3.47 ‰ to 5.09 ‰ in bivalve shells and reach values down to −21.43 ‰ and −4.67 ‰ for the carbonate nodule matrix and embedded bivalve shells (sample POL-29), respectively. Using the Δ_{47}-derived temperature to estimate the oxygen isotope fractionation factor results in $\delta^{18}O_w$ values ranging from −4.88 ± 1.20 ‰ to −2.52 ± 0.78 ‰ in Siberian bivalves. A much lower value of −10.6 ± 0.9 ‰ is obtained for the fracture-infilling calcite vein from the Polovinnaya River.

4.2 Warcq, France

Mollusc shells from Warcq showing an aragonite mineralogy revealed microstructures similar to those observed in *Dacryomya jacutica* from Siberia, the main differences being that sheet nacreous structures of the studied ammonite shell (ARD-05) show thinner tablets than those of bivalve shells (Fig. 3). Both SEM and Raman data indicate that the sample ARD-03 (bivalve fragment) is in calcite, showing a darker colour and no iridescence, with a much simpler and massive structure observed in SEM (Fig. 3).

The Δ_{47} values of measured bivalve and ammonite shells from Warcq range from 0.5851 ± 0.0095 ‰ to 0.5955 ± 0.0130 ‰ I-CDES. Reconstructed Δ_{47} temperatures range from 24.4 ± 4.4 to 28.0 ± 3.3 °C. Mean $\delta^{18}O_c$ values are −2.30 ± 0.76 ‰ (1 SD, $n = 6$, max = −0.83 ‰, min = −2.79 ‰), and $\delta^{13}C$ ranges from 0.37 ‰ to 2.82 ‰. The calculated $\delta^{18}O_w$ values range from 0.6 ± 0.7 ‰ to −1.4 ± 1.0 ‰.

5 Discussion

5.1 Sample preservation

The SEM and Raman observations reveal that the analysed mollusc shells from both sites retain pristine aragonite mineralogy and microstructures with evidence of neither recrystallization nor mineralogical conversion (Fig. 3). Despite their aragonite mineralogy, the *Dacryomya* shells from sample POL-29 record unusually low $\delta^{13}C$ values that are ∼ 8 ‰ lower than the other *Dacryomya* shells analysed from the same succession. The carbonate matrix of the nodule where these shells are embedded also records a very low $\delta^{13}C$ value (−21.43 ‰) but a $\delta^{18}O$ value within the range of the bivalve shells. We therefore attribute the extremely low $\delta^{13}C$ values of bivalves shells of this level to an early diagenetic phase resulting in the formation of carbonate nodules derived from respiratory CO_2 that locally altered the bivalve shell geochemistry.

Organic matter maturity, mineralogical, and sedimentological data all imply exceptionally shallow burial depth (< 1 km) for the samples investigated here. Maximum burial temperature (T_{burial}) remained well below the commonly assumed minimum temperature (80–120 °C) of solid-state reordering of C–O bonds in calcite at geological timescales (Henkes et al., 2014; Stolper and Eiler, 2015; Hemingway and Henkes, 2021). Recent experiments show that aragonite is more susceptible to solid-state bond reordering (Chen et al., 2019), but to our knowledge there is no existing model constraining the temperatures at which this process would markedly overwrite the Δ_{47} value of this mineral at such timescales. The exceptional preservation of aragonite nacre-

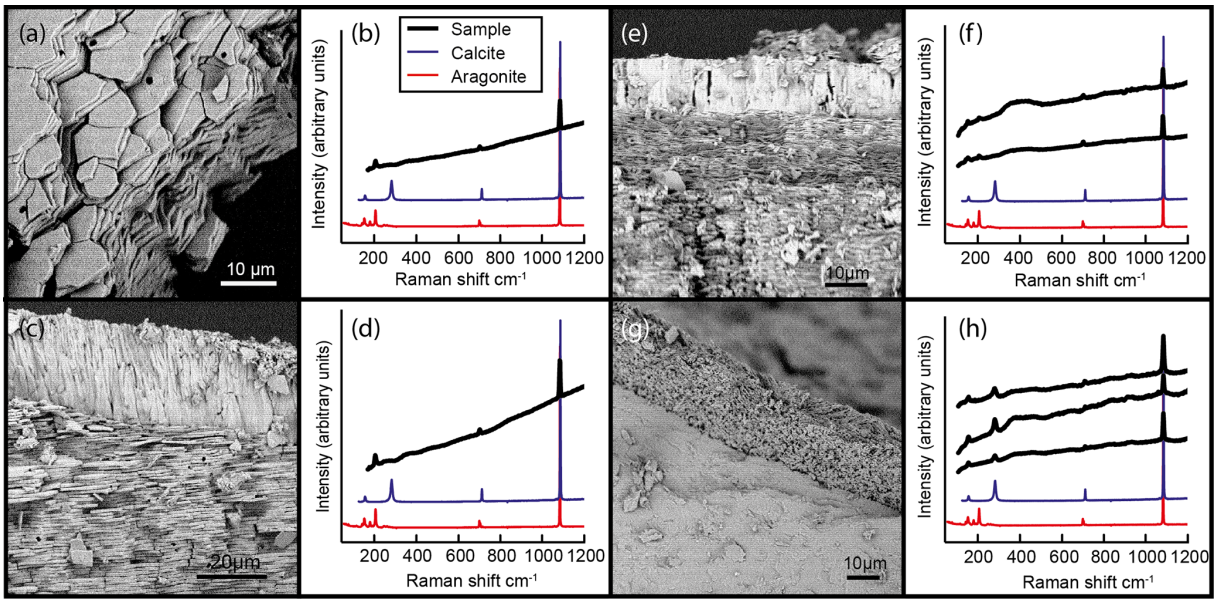

Figure 3. SEM images and Raman spectra for a selection of samples. (**a**, **c**, **e**, and **g**) SEM images of samples POL-8, POL-12, ARD-05, and ARD-03, respectively. (**b**, **d**, **f**, and **g**) Raman spectra of samples POL-8, POL-12, ARD-05, and ARD-03 compared to the reference spectra of calcite and aragonite.

ous sheet microstructures in these samples implies minimal amounts of fluid circulation and recrystallization, if any. Exchange between fluid inclusions in mollusc shells and the surrounding carbonate minerals was recently suggested as an alternative process that may alter the clumped isotope signature of biogenic carbonates without substantially affecting the stable isotope signature of the shell or its mineralogy (Nooitgedacht et al., 2021). In heating experiments, these exchanges resulted in a significant decrease in the Δ_{47} value of the bivalve shells compared to the original shell and a minor (~ 0.1 ‰) decrease in $\delta^{18}O$ of the heated shell. We cannot exclude the possibility that this process has altered the fossils studied here even at low temperature, nor do we have evidence that it occurred. The Δ_{47} temperature of 31.1 ± 4.8 °C for the fracture-infilling calcite vein in Arctic Russia is significantly higher than those inferred from bivalves and is consistent with a formation depth < 1 km assuming a geothermal gradient of 25 °C km^{-1}. The reconstructed $\delta^{18}O_w$ value of -10.7 ± 0.9 ‰ for this calcite vein is also substantially lower than those inferred from associated bivalves, consistent with a late-phase meteoric source for the mineralizing fluid. The precise depth and date at which this vein formed, however, remain uncertain.

Based on the geological setting of the samples and their preservation, we consider any substantial alteration of their original geochemical signature unlikely. In the remote scenario that the studied material has been slightly modified by solid-state bond reordering, one would expect the Δ_{47} of the samples to be lower than their original values (Henkes et al., 2014; Stolper and Eiler, 2015; Fernandez et al., 2021; Hemingway and Henkes, 2021). Therefore, both the temperature and $\delta^{18}O_w$ reported here would be overestimated and should be taken as an upper limit of original environmental parameters.

5.2 Evidence for extreme warmth and reduced salinity in the Arctic during the Toarcian Oceanic Anoxic Event (T-OAE)

Bivalve shells record a marked rise in $\delta^{13}C$ along the section up to ~ 5 ‰ that parallels that recorded by organic carbon $\delta^{13}C$ data (Fig. 4; Suan et al., 2011). These results strengthen the correlation of the corresponding part of the succession with the rising limb of the positive carbon isotope excursion commonly used to characterize the termination of the T-OAE interval at coeval sites in Europe and North Africa (Jenkyns and Clayton, 1986; Suan et al., 2010; Krencker et al., 2014; Baghli et al., 2020; Ullmann et al., 2020). Bivalve shell $\delta^{18}O_c$ values, however, show no stratigraphic trend as opposed to brachiopod shell T-OAE records from the western Tethys at mid-latitudes (Suan et al., 2010; Krencker et al., 2014; Baghli et al., 2020; Ullmann et al., 2020). Our Δ_{47} results yield polar temperatures ranging from 8.8 ± 5.2 to 18.0 ± 3.4 °C (mean = 14.7 °C). As occurs with most Δ_{47}-derived temperature datasets, the relatively large uncertainties of the present estimates of Siberian sea surface temperature (SST) hamper the identification of distinctive stratigraphic trends.

Bivalve shell growth can be highly variable during the animal's life (Schöne, 2008), making any paleoenvironmental record derived from the bivalve shell either incomplete (because of growth cessation) or at least biased towards the

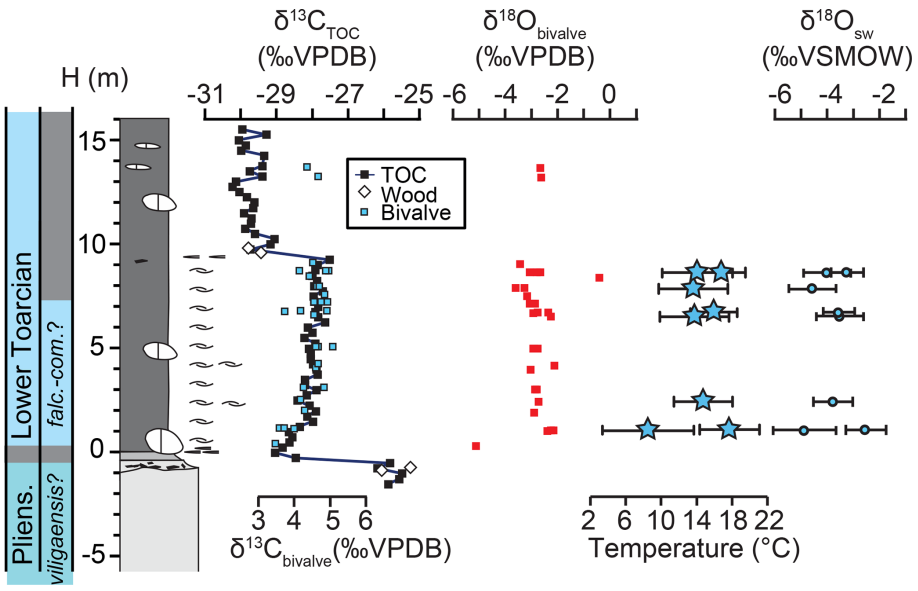

Figure 4. Geochemical record of the T-OAE at the Polovinnaya River, Arctic Siberia. Stratigraphy and biostratigraphic zones are for the Arctic realm (falc.: falciferum zone, com.: commune zone). The organic carbon isotope ($\delta^{13}C_{TOC}$) data (black squares) and wood debris $\delta^{13}C$ data (white diamonds) are from Suan et al. (2011); the bivalve shell $\delta^{13}C$ data (blue squares), bivalve shell $\delta^{18}O$ (red squares), Δ_{47} temperatures (blue stars), and $\delta^{18}O_w$ estimates (blue circles) inferred from bivalve shell Δ_{47} values are from this study. The analysed bivalve samples all belong to the species *Dacryomya jacutica*. Δ_{47}-derived temperatures were computed using the equation of Anderson et al. (2021). $\delta^{18}O_w$ was calculated using the oxygen isotope fractionation equation of Grossman and Ku (1986).

period of maximum growth rate. Shell growth rate can be controlled by environmental parameters (temperature, salinity, food availability), biological processes such as spawning, and changes during the ontogeny (Schöne, 2008). One major aspect of shell growth that may bias the geochemical signal data is seasonal shell growth cessation. In modern high-latitude bivalves, seasonal shell growth cessation generally occurs during the winter, triggered by low temperatures or low food availability (Peck et al., 2000; Vihtakari et al., 2016; Killam and Clapham, 2018). In the present-day *Nucula annulata*, an aragonite bivalve with ecology similar to the analysed *Dacryomya jacutica*, growth cessation occurs in winter and during spawning at peak local temperatures, with its average $\delta^{18}O_c$ hence recording late spring to early fall SST (Craig, 1994). By contrast, growth band $\delta^{18}O_c$ offers evidence for summertime-only growth cessation in high-latitude Eocene bivalves from Antarctica, with inferred winter SST of 11.1 ± 0.6 and summer SST of 17.6 ± 1.3 °C (Buick and Ivany, 2004; Douglas et al., 2014). A comparable seasonal $\delta^{18}O_c$ record could not be generated from our Russian Arctic material owing to the very small size of the available *Dacryomya* shells (1 to 2 cm). In any case, the temperate data from NE France should be minimally affected by seasonal biases as shell precipitation occurs more continuously throughout the year in modern temperate molluscs (Killam and Clapham, 2018). Besides, both sites were deposited in nearshore environments at very shallow depths likely not exceeding a few tens of metres (Suan et al., 2011; Thuy et al., 2011). Although bivalves from both sections record temperatures near the sea bottom that were likely slightly cooler than the sea surface, the difference should not have exceeded a few degrees; owing to their shallow living depth we expect the studied bivalves to have lived within the thermocline. We therefore conservatively interpret the reconstructed temperatures as reflecting polar warm-season SST (summer; SST_{PWS}) in Arctic Russia and low-latitude annual SST in NE France. These SST_{PWS} values for the T-OAE are still 10–20 °C higher than present-day SST_{PWS} (Fig. 5).

The reconstructed polar $\delta^{18}O_w$ values ranging from -4.9 ± 1.2‰ to -2.5 ± 0.8‰ VSMOW during the T-OAE are significantly lower than the value of -1‰ VSMOW expected for an ice-free world mean open ocean (Shackleton and Kennett, 1975). These results imply a substantial freshwater contribution to the studied basin during the T-OAE, probably resulting from coastal runoff at this relatively proximal site (Suan et al., 2011). High temperatures and reduced salinity are in broad agreement with paleontological evidence for warm and humid temperate conditions during the T-OAE interval in Arctic Siberia (Rogov et al., 2019). Brackish conditions are also consistent with the fossil assemblages of the succession that includes abundant terrestrial organic matter and wood debris, marine to brackish elements such as abundant dinoflagellate cysts, benthic foraminifera (preserved as organic linings and agglutinate forms), and typically marine elements that are represented by a few belemnite rostra and unidentifiable ammonite in-

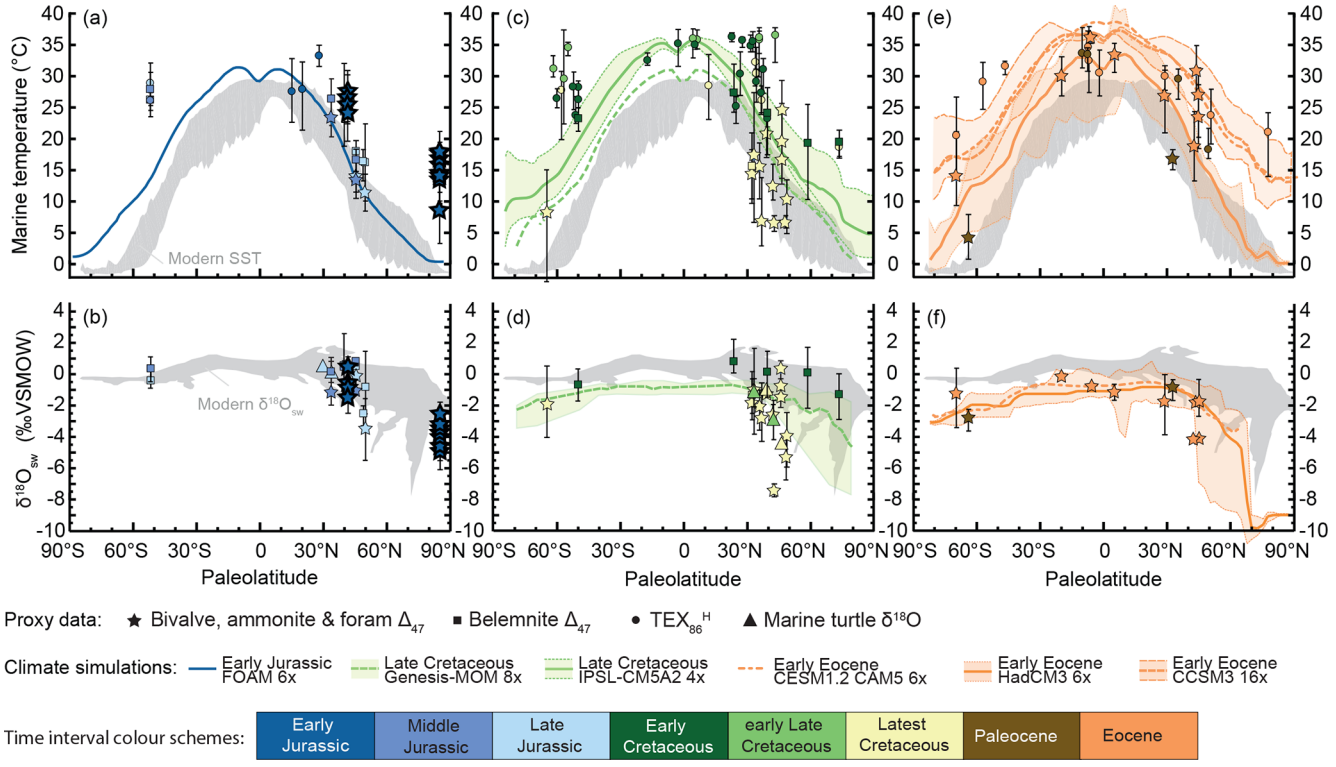

Figure 5. Comparison of the new (bold outline) reconstructed Early Jurassic SST and $\delta^{18}O_{sw}$ with published Jurassic–Eocene proxy-based reconstructions (thin outline) and Earth system simulations. Proxy–model comparisons of SST and $\delta^{18}O_{sw}$ are shown for the Jurassic **(a, b)**, the Cretaceous **(c, d)**, and the early Paleogene **(e, f)**. Proxy data are divided between eight time slices based on their definition in the International Chronostratigraphic Chart v2020/03 (Cohen et al., 2013; updated); early Late Cretaceous: Cenomanian to Santonian; latest Cretaceous: Campanian–Maastrichtian. Marker colour shows sample age accordingly (see key). New data are displayed as the reported value and its associated uncertainties for each samples. Datasets from the literature, from the same proxy and location, were regrouped within each time slice. The marker displays the mean of available data and the error bar the extent of the data (minimal to maximal value). Both Δ_{47} and TEX_{86}^{H} temperatures are published temperatures. $\delta^{18}O_w$ values were recomputed using published Δ_{47} temperatures and $\delta^{18}O_c$ with the following fractionation equations – belemnite calcite: Coplen, (2007), aragonite: Grossman and Ku(1986), bivalve calcite: Epstein et al. (1953), foraminifera: Erez and Luz (1983), turtle bones: Barrick et al. (1999), updated by Pouech et al. (2014). Results of Earth system simulations from the literature are shown as annual averages (bold lines) and summer and winter seasonal averages (colour shading). Modern ranges of SST and $\delta^{18}O_{sw}$ are also shown (grey shading) for comparison. Δ_{47} data are from the following: Keating-Bitonti et al., 2011; Douglas et al., 2014; Petersen et al., 2016b, a; Evans et al., 2018; Wierzbowski et al., 2018; Meyer et al., 2018; Vickers et al., 2019, 2020, 2021; Price et al., 2020; Brigaud et al., 2020; Fernandez et al., 2021; de Winter et al., 2021. TEX_{86}^{H} paleothermometry data are from the following: Jenkyns et al., 2012; Lunt et al., 2012; Douglas et al., 2014; Frieling et al., 2014; O'Brien et al., 2017; Robinson et al., 2017; Cramwinckel et al., 2018; O'Connor et al., 2019; Ruebsam et al., 2020; Cavalheiro et al., 2021 . Marine turtle phosphate $\delta^{18}O$ data are from Billon-Bruyat et al. (2005), Coulson et al. (2011), and van Baal et al. (2013). The FOAM 6× simulation is from Dera and Donnadieu (2012), the Genesis-MOM 8× simulation is from Zhou et al. (2008), IPSL-CM5A2 4× is from Laugié et al. (2020), CESMA.2 CAM5 6× is from Zhu et al. (2020), HadCM3 6× is from Tindall et al. (2010), and CCSM3 16× is from Huber and Caballero (2011), with Nx indicating CO_2 levels used in the simulations as a multiple of pre-industrial level (i.e. 280 ppm). More detailed information on the building of this figure and the data compilation is available in the Supplement.

ternal moulds (Suan et al., 2011). Interestingly, protobranch bivalves, to which *Dacryomya* belongs, are not well adapted to salinities lower than 20 ‰ (Zardus, 2002). Assuming a similar lower salinity limit for Polovinnaya River bivalves, a global mean ocean with a salinity of 34.5 ‰, and a $\delta^{18}O_w$ of −1 ‰ VSMOW, mass balance considerations (see the Supplement) imply an upper limit of ∼ −8 ‰ VSMOW for local $\delta^{18}O$ of precipitation and runoff ($\delta^{18}O_p$). This value is high relative to modern Arctic $\delta^{18}O_p$ but in agreement with the prediction that higher polar temperatures should have produced higher $\delta^{18}O_p$ than those prevailing today (Rozanski et al., 1992). Similarly, terrestrial plant *n*-alkane hydrogen isotopes and paleosol siderite Δ_{47} data indicate slightly lower Arctic $\delta^{18}O_p$ of −10 ‰ to −15 ‰ VSMOW during the early Eocene (Pagani et al., 2006; van Dijk et al., 2020), another well-established warm period with evidence of polar warmth (Markwick, 1998; Sluijs et al., 2006, 2020; Douglas et al., 2014; Suan et al., 2017; van Dijk et al., 2020). As-

suming a similar range of $\delta^{18}O_p$ values in the Early Jurassic Arctic and the assumption listed above for the Early Jurassic oceans, mass balance calculations indicate mean salinity of 23.9 ± 2.9 ‰ (1σ, $n = 8$) and 27.7 ± 1.8 ‰ (1σ, $n = 8$) with $\delta^{18}O_p$ of -10 ‰ and -15 ‰ VSMOW, respectively (see the Supplement), again consistent with paleontological evidence suggesting brackish waters at the Polovinnaya River during the Toarcian. Such values are also comparable to the salinity of 28 ‰ estimated using a fully coupled ocean–atmosphere model for the Toarcian (Dera and Donnadieu, 2012), although the Arctic temperatures obtained by the same model are in strong disagreement with our data (Fig. 5). Such observations should be replicated around the Arctic realm to test whether the brackish environment evidenced here was of local or more regional nature.

5.3 Early Jurassic latitudinal temperature and $\delta^{18}O_w$ gradients

The mid-paleolatitude SSTs reconstructed by our new clumped isotope data (~ 25 °C) are in good agreement with recent Sinemurian–Pliensbachian and Toarcian TEX_{86}^H data pointing to summer SST $\sim$ 20–30 °C at slightly lower paleolatitudes (Robinson et al., 2017; Ruebsam et al., 2020). It should be noted that the mid-latitude samples presented here are from the Davoei zone and predate the T-OAE interval recorded by the Siberian data by ~ 6 million years. Nevertheless, climate proxies from the Davoei zone indicate that the corresponding time interval, although likely slightly cooler than the T-OAE, corresponds to one of the warmest periods of the Early Jurassic (Dera et al., 2011; Bougeault et al., 2017). The new clumped isotope data from the two sites, even if they are not strictly contemporaneous, can therefore be reasonably used to tentatively estimate latitudinal gradient during the warmest episodes of the Early Jurassic. The Δ_{47} data presented herein suggest a decrease in mean SST of 0.26 ± 0.05 °C per degree of latitude between middle and high latitudes, i.e. a reduction of the latitudinal SST gradient of 32 ± 10 % relative to present, consistent with the most conservative early Eocene estimates (Evans et al., 2018). Comparing our Siberian T-OAE Δ_{47} temperatures with contemporaneous TEX_{86}^H temperatures estimated for low latitudes (Ruebsam et al., 2020) results in an even shallower gradient of 0.17 ± 0.05 °C per degree of latitude between low and high latitudes.

Considering the scarcity of other Early Jurassic temperature proxy data, model-based SST, and $\delta^{18}O_w$ estimates, we extend the comparison to SST and $\delta^{18}O_w$ estimates based on various proxy data and published Earth system simulations for other Jurassic to Eocene intervals (Fig. 5; Supplement). First, the new Δ_{47} temperatures can be compared with other well-established warm intervals, such as the Cenomanian–Turonian and the Eocene. The compilation shows that Δ_{47} SSTs from NE France agree with most previous mid-latitude TEX_{86}^H and Δ_{47} SSTs for the Eocene interval (20–30 °C), with values > 5 °C higher than present-day SST. Mid-latitude Cenomanian–Turonian TEX_{86}^H SSTs are significantly higher (> 30 °C) and form the highest mid-latitude temperature of the compilation. High-latitude data are much more scarce. Still, Russian Arctic Toarcian SSTs are very close to early Eocene polar SST derived from Arctic (Sluijs et al., 2006, 2020; Suan et al., 2010) and Antarctic (Douglas et al., 2014) sites, with polar SST > 15 °C warmer than present during these two distinct greenhouse periods (Fig. 5).

Our Δ_{47} SST for the Lower Jurassic can be compared to published results from Earth system models that simulate these intervals of global warmth (see previous paragraph) to discuss model–data discrepancies, especially apparent at high latitudes. Proxy data indicate an atmospheric pCO_2 of 1000 ± 500 ppmv during the Early Jurassic, with maximum values of 1750 ± 500 ppmv, i.e. 6× pre-industrial levels (PILs), during the T-OAE (McElwain et al., 2005; Li et al., 2020). Earth system models run at 6× PIL for the Early Jurassic (Dera and Donnadieu, 2012) or Cretaceous–Eocene paleogeography almost invariably produce lower SSTs than those inferred from our Δ_{47} data, with a maximum model–data discrepancy of > 15 °C at high latitudes (Fig. 5). To achieve such polar warmth, the Eocene CCSM3 simulations require 16× PIL, which is more than twice that indicated by Lower Jurassic and Eocene proxy data (Huber and Caballero, 2011). Reconstructed SSTs of 14.4 ± 2.8 °C near the North Pole during the T-OAE, however, correspond to the maximum monthly temperatures simulated by the Turonian IPSL-CM5A2 model near the North Pole at 4× PIL (Laugié et al., 2020). The hypothesis of shell growth restricted to the warmest month in the analysed Toarcian Arctic bivalves, however, remains questionable given the evidence for summertime-only growth cessation in Eocene bivalves from Antarctica (Buick and Ivany, 2004). Finally, Arctic SSTs as high as 15–20 °C are successfully achieved in the Eocene CESM1.2 CAM5 at 6 to 9× PIL (Zhu et al., 2020), in which climate sensitivity increases with rising CO_2 due to low-altitude cloud albedo feedbacks and improved radiative parameterization. As this model produces an increase in climate sensitivity with CO_2 in both Eocene and modern conditions, our results thus support the growing body of evidence that the amplitude of future anthropogenic warming may be underestimated by conventional state-of-the-art models.

The reconstruction of $\delta^{18}O_w$ values using proxy data provides a complementary aspect to assess model capabilities, as this indicator is sensitive to both climate parameters (moisture, humidity, and temperatures) and paleogeography. Our mid-latitude $\delta^{18}O_w$ values are broadly similar to those reconstructed using marine turtle bone $\delta^{18}O_{PO_4}$ and Δ_{47} data from Jurassic to Eocene bivalves, ammonites, and foraminifera (Fig. 5, Billon-Bruyat et al., 2005; Coulson et al., 2011; van Baal et al., 2013; Evans et al., 2018; Wierzbowski et al., 2018; Vickers et al., 2021; de Winter et al., 2021). The reconstructed $\delta^{18}O_w$ values are, to some extent, also broadly

comparable with those inferred from belemnite calcite Δ_{47} data (Wierzbowski et al., 2018; Vickers et al., 2019, 2020, 2021; Price et al., 2020), although such data should be interpreted with caution owing to the likely unique oxygen isotope fractionation of belemnite calcite (Price et al., 2020; Vickers et al., 2021). In line with evidence for substantial ^{18}O depletion of Toarcian Arctic waters (relative to VSMOW) suggested by our data, previous studies suggested low $\delta^{18}O_w$ values in interior seas bordered by large continental areas, such as in the Western Interior Seaway during the Campanian–Maastrichtian (Coulson et al., 2011; Petersen et al., 2016b; Meyer et al., 2018) and the Middle Russian Sea during the Middle to Late Jurassic interval (Wierzbowski et al., 2018). Interestingly, the Δ_{47} temperatures reported in these basins also differ markedly from those reported in more open-ocean sites of similar age and paleolatitude, suggesting the possible influence of colder Arctic water masses through southward ocean currents. Indeed, the Middle to Late Jurassic Δ_{47} temperatures reported in the Middle Russian Sea (Wierzbowski et al., 2018) are $\sim 10\,°C$ lower than coeval data from the Hebrides basin, Scotland (Vickers et al., 2020), and from the high mid-latitude Falkland Plateau in the Southern Hemisphere (Vickers et al., 2019). Such anomalies in $\delta^{18}O_w$ values and temperatures demonstrate the importance of regional patterns such as river runoff and basin connections on the environmental parameters of a restricted basin (Petersen et al., 2016b). More generally, local anomalies in $\delta^{18}O_w$ values evidenced by the new and earlier clumped isotope data highlight the ability of this proxy to decipher the influence of the temperature and $\delta^{18}O_w$ values in otherwise similar $\delta^{18}O_c$ datasets.

We are aware of only three Earth system $\delta^{18}O_w$ simulations for the broad time interval considered here (Zhou et al., 2008; Tindall et al., 2010; Zhu et al., 2020), hence limiting model–data comparisons. The higher freshwater contribution near high-latitude land masses of the Northern Hemisphere in all these models produced lower $\delta^{18}O_w$ values that are broadly consistent with previous data and our proxy data (Fig. 5). This good agreement, however, might be partly fortuitous, as proxy data suggest SSTs much higher than those produced by these models (Fig. 5). As mentioned above (section 5.2), such higher-than-predicted polar warmth would have substantially increased high-latitude $\delta^{18}O_p$ so that higher runoff would be required to reproduce the magnitude of the poleward drop in $\delta^{18}O_w$ indicated by proxy data. This highlights the usefulness, in future models of past greenhouse climates, of systematically providing $\delta^{18}O_w$ predictions so that $\delta^{18}O_w$ estimates derived from Δ_{47} data may serve as a constraint on Earth system models.

6 Conclusions

The clumped isotope compositions of pristine, minimally buried, marine mollusc shells yield SST $> 25\,°C$ at mid-latitudes during the early Pliensbachian and SST $> 10\,°C$ at polar paleolatitudes during the T-OAE. The reconstructed $\delta^{18}O_w$ values point to a higher freshwater contribution toward Arctic regions, illustrating the dangers of assuming a fixed global $\delta^{18}O_w$ value for $\delta^{18}O$-derived temperature reconstructions. Although further work should clarify the influence of seasonal changes in the recorded SST values at polar sites, these results strengthen a growing body of evidence for higher climate sensitivity under high atmospheric CO_2 conditions and suggest that this higher sensitivity has been a general feature of greenhouse climates since at least 180 Ma.

Data availability. Detailed data supporting this study are available in the Supplement. Raw data are available on request to the author.

Supplement. The supplement related to this article is available online at: https://doi.org/10.5194/cp-18-435-2022-supplement.

Author contributions. TL and GS designed the study and led the writing in close cooperation with CL, MR, and MD. MR and GS participated in the fieldwork and collected the samples. TL prepared and sampled the shell material for geochemistry and performed the SEM observations. MR, JS, and OL identified the fossils. MD and TL performed the clumped isotope analyses and data processing. AVL and TL performed the stable isotopes analyses and data processing. BR, GM, and TL gathered and interpreted the Raman spectra. TL and GS compiled the paleotemperature proxy database. All authors were involved in the interpretation of the results.

Competing interests. The contact author has declared that neither they nor their co-authors have any competing interests.

Disclaimer. Publisher's note: Copernicus Publications remains neutral with regard to jurisdictional claims in published maps and institutional affiliations.

Acknowledgements. We thank Ghislaine Broillet for her help with SEM analyses and Ophélie Lodyga for her help with Raman analyses. We thank two anonymous reviewers for their constructive suggestions and comments that substantially improved the paper.

Financial support. This research has been supported by the Agence Nationale de la Recherche through ANR OXYMORE (grant no. ANR-18-CE31-0020) as well as joint CNRS/RFBR International Emerging Action grants from the Centre National de la Recherche Scientifique (CNRS; grant no. 205700), Russian Foundation for Basic Research (RFBR; grant no. 21-55-15015), and Slovak Research and Development Agency (grant no. APVV 17-0555 to Jan Schlögl).

Review statement. This paper was edited by Luc Beaufort and reviewed by two anonymous referees.

References

Anderson, N. T., Kelson, J. R., Kele, S., Daëron, M., Bonifacie, M., Horita, J., Mackey, T. J., John, C. M., Kluge, T., Petschnig, P., Jost, A. B., Huntington, K. W., Bernasconi, S. M., and Bergmann, K. D.: A unified clumped isotope thermometer calibration (0.5–1100 °C) using carbonate-based standardization, Geophys. Res. Lett., 38, e2020GL092069, https://doi.org/10.1029/2020GL092069, 2021.

Baghli, H., Mattioli, E., Spangenberg, J. E., Bensalah, M., Arnaud-Godet, F., Pittet, B., and Suan, G.: Early Jurassic climatic trends in the south-Tethyan margin, Gondwana Res., 77, 67–81, https://doi.org/10.1016/j.gr.2019.06.016, 2020.

Barrick, R. E., Fischer, A. G., and Showers, W. J.: Oxygen isotopes from turtle bone; applications for terrestrial paleoclimates?, PALAIOS, 14, 186–191, https://doi.org/10.2307/3515374, 1999.

Bernasconi, S. M., Müller, I. A., Bergmann, K. D., Breitenbach, S. F. M., Fernandez, A., Hodell, D. A., Jaggi, M., Meckler, A. N., Millan, I., and Ziegler, M.: Reducing Uncertainties in Carbonate Clumped Isotope Analysis Through Consistent Carbonate-Based Standardization, Geochem. Geophy. Geosy., 19, 2895–2914, https://doi.org/10.1029/2017GC007385, 2018.

Bernasconi, S. M., Daëron, M., Bergmann, K. D., Bonifacie, M., Meckler, A. N., Affek, H. P., Anderson, N., Bajnai, D., Barkan, E., Beverly, E., Blamart, D., Burgener, L., Calmels, D., Chaduteau, C., Clog, M., Davidheiser-Kroll, B., Davies, A., Dux, F., Eiler, J., Elliott, B., Fetrow, A. C., Fiebig, J., Goldberg, S., Hermoso, M., Huntington, K. W., Hyland, E., Ingalls, M., Jaggi, M., John, C. M., Jost, A. B., Katz, S., Kelson, J., Kluge, T., Kocken, I. J., Laskar, A., Leutert, T. J., Liang, D., Lucarelli, J., Mackey, T. J., Mangenot, X., Meinicke, N., Modestou, S. E., Müller, I. A., Murray, S., Neary, A., Packard, N., Passey, B. H., Pelletier, E., Petersen, S., Piasecki, A., Schauer, A., Snell, K. E., Swart, P. K., Tripati, A., Upadhyay, D., Vennemann, T., Winkelstern, I., Yarian, D., Yoshida, N., Zhang, N., and Ziegler, M.: InterCarb: A Community Effort to Improve Interlaboratory Standardization of the Carbonate Clumped Isotope Thermometer Using Carbonate Standards, Geochem. Geophy. Geosy., 22, e2020GC009588, https://doi.org/10.1029/2020GC009588, 2021.

Billon-Bruyat, J.-P., Lécuyer, C., Martineau, F., and Mazin, J.-M.: Oxygen isotope compositions of Late Jurassic vertebrate remains from lithographic limestones of western Europe: implications for the ecology of fish, turtles, and crocodilians, Palaeogeogr. Palaeocl., 216, 359–375, https://doi.org/10.1016/j.palaeo.2004.11.011, 2005.

Blaise, T., Barbarand, J., Kars, M., Ploquin, F., Aubourg, C., Brigaud, B., Cathelineau, M., El Albani, A., Gautheron, C., Izart, A., Janots, D., Michels, R., Pagel, M., Pozzi, J.-P., Boiron, M.-C., and Landrein, P.: Reconstruction of low temperature (< 100 °C) burial in sedimentary basins: A comparison of geothermometer in the intracontinental Paris Basin, Mar. Petrol. Geol., 53, 71–87, https://doi.org/10.1016/j.marpetgeo.2013.08.019, 2014.

Bougeault, C., Pellenard, P., Deconinck, J.-F., Hesselbo, S. P., Dommergues, J.-L., Bruneau, L., Cocquerez, T., Laffont, R., Huret, E., and Thibault, N.: Climatic and palaeoceanographic changes during the Pliensbachian (Early Jurassic) inferred from clay mineralogy and stable isotope (C-O) geochemistry (NW Europe), Glob. Planet. Change, 149, 139–152, https://doi.org/10.1016/j.gloplacha.2017.01.005, 2017.

Brigaud, B., Bonifacie, M., Pagel, M., Blaise, T., Calmels, D., Haurine, F., and Landrein, P.: Past hot fluid flows in limestones detected by Δ_{47}–(U-Pb) and not recorded by other geothermometers, Geology, 48, 851–856, https://doi.org/10.1130/G47358.1, 2020.

Buick, D. P. and Ivany, L. C.: 100 years in the dark: Extreme longevity of Eocene bivalves from Antarctica, Geology, 32, 921–924, https://doi.org/10.1130/G20796.1, 2004.

Cavalheiro, L., Wagner, T., Steinig, S., Bottini, C., Dummann, W., Esegbue, O., Gambacorta, G., Giraldo-Gómez, V., Farnsworth, A., Flögel, S., Hofmann, P., Lunt, D. J., Rethemeyer, J., Torricelli, S., and Erba, E.: Impact of global cooling on Early Cretaceous high pCO_2 world during the Weissert Event, Nat. Commun., 12, 5411, https://doi.org/10.1038/s41467-021-25706-0, 2021.

Chen, S., Ryb, U., Piasecki, A. M., Lloyd, M. K., Baker, M. B., and Eiler, J. M.: Mechanism of solid-state clumped isotope reordering in carbonate minerals from aragonite heating experiments, Geochim. Cosmochim. Ac., 258, 156–173, https://doi.org/10.1016/j.gca.2019.05.018, 2019.

Cohen, K. M., Finney, S. C., Gibbard, P. L., and Fan, J.-X.: The ICS International Chronostratigraphic Chart, Episodes, 36, 199–204, https://doi.org/10.18814/epiiugs/2013/v36i3/002, 2013.

Coplen, T. B.: Calibration of the calcite–water oxygen-isotope geothermometer at Devils Hole, Nevada, a natural laboratory, Geochim. Cosmochim. Ac., 71, 3948–3957, https://doi.org/10.1016/j.gca.2007.05.028, 2007.

Coulson, A. B., Kohn, M. J., and Barrick, R. E.: Isotopic evaluation of ocean circulation in the Late Cretaceous North American seaway, Nat. Geosci., 4, 852–855, https://doi.org/10.1038/ngeo1312, 2011.

Craig, N.: Growth of the bivalve Nucula annulata in nutrient-enriched environments, Mar. Ecol. Prog. Ser., 104, 77–90, https://doi.org/10.3354/meps104077, 1994.

Cramwinckel, M. J., Huber, M., Kocken, I. J., Agnini, C., Bijl, P. K., Bohaty, S. M., Frieling, J., Goldner, A., Hilgen, F. J., Kip, E. L., Peterse, F., van der Ploeg, R., Röhl, U., Schouten, S., and Sluijs, A.: Synchronous tropical and polar temperature evolution in the Eocene, Nature, 559, 382–386, https://doi.org/10.1038/s41586-018-0272-2, 2018.

Daëron, M.: Full Propagation of Analytical Uncertainties in Δ_{47} Measurements, Geochem. Geophy. Geosy., 22, https://doi.org/10.1029/2020GC009592, 2021.

Daëron, M., Blamart, D., Peral, M., and Affek, H. P.: Absolute isotopic abundance ratios and the accuracy of Δ_{47} measurements, Chem. Geol., 442, 83–96, https://doi.org/10.1016/j.chemgeo.2016.08.014, 2016.

de Winter, N. J., Müller, I. A., Kocken, I. J., Thibault, N., Ullmann, C. V., Farnsworth, A., Lunt, D. J., Claeys, P., and Ziegler, M.: Absolute seasonal temperature estimates from clumped isotopes in bivalve shells suggest warm and variable greenhouse climate, Commun. Earth Environ., 2, 121, https://doi.org/10.1038/s43247-021-00193-9, 2021.

Dera, G. and Donnadieu, Y.: Modeling evidences for global warming, Arctic seawater freshening, and sluggish oceanic circulation during the Early Toarcian anoxic event, Paleoceanography, 27, PA2211, https://doi.org/10.1029/2012PA002283, 2012.

Dera, G., Pucéat, E., Pellenard, P., Neige, P., Delsate, D., Joachimski, M. M., Reisberg, L., and Martinez, M.: Water mass exchange and variations in seawater temperature in the NW Tethys during the Early Jurassic: Evidence from neodymium and oxygen isotopes of fish teeth and belemnites, Earth Planet. Sc. Lett., 286, 198–207, https://doi.org/10.1016/j.epsl.2009.06.027, 2009.

Dera, G., Brigaud, B., Monna, F., Laffont, R., Pucéat, E., Deconinck, J.-F., Pellenard, P., Joachimski, M. M., and Durlet, C.: Climatic ups and downs in a disturbed Jurassic world, Geology, 39, 215–218, https://doi.org/10.1130/G31579.1, 2011.

Disnar, J. R., Le Strat, P., Farjanel, G., and Fikri, A.: Sédimentation de la matière organique dans le nord-est du Bassin de Paris: conséquences sur le dépôt des argilites carbonées du Toarcien inférieur (Organic matter sedimentation in the northeast of the Paris Basin: consequences on the deposition of the lower toarcian black shales), Chem. Geol., 131, 15–35, https://doi.org/10.1016/0009-2541(96)00021-6, 1996.

Douglas, P. M. J., Affek, H. P., Ivany, L. C., Houben, A. J. P., Sijp, W. P., Sluijs, A., Schouten, S., and Pagani, M.: Pronounced zonal heterogeneity in Eocene southern high-latitude sea surface temperatures, P. Natl. Acad. Sci. USA, 111, 6582–6587, https://doi.org/10.1073/pnas.1321441111, 2014.

Epstein, S., Buchsbaum, R., Lowenstam, H. A., and Urey, H. C.: Revised carbonate-water isotopic temperature scale, Geol. Soc. Am. Bull., 64, 1315, https://doi.org/10.1130/0016-7606(1953)64[1315:RCITS]2.0.CO;2, 1953.

Erez, J. and Luz, B.: Experimental paleotemperature equation for planktonic foraminifera, Geochim. Cosmochim. Ac., 47, 1025–1031, https://doi.org/10.1016/0016-7037(83)90232-6, 1983.

Evans, D., Sagoo, N., Renema, W., Cotton, L. J., Müller, W., Todd, J. A., Saraswati, P. K., Stassen, P., Ziegler, M., Pearson, P. N., Valdes, P. J., and Affek, H. P.: Eocene greenhouse climate revealed by coupled clumped isotope-Mg/Ca thermometry, P. Natl. Acad. Sci. USA, 115, 1174–1179, https://doi.org/10.1073/pnas.1714744115, 2018.

Fernandez, A., Korte, C., Ullmann, C. V., Looser, N., Wohlwend, S., and Bernasconi, S. M.: Reconstructing the magnitude of Early Toarcian (Jurassic) warming using the reordered clumped isotope compositions of belemnites, Geochim. Cosmochim. Ac., 293, 308–327, https://doi.org/10.1016/j.gca.2020.10.005, 2021.

Frieling, J., Iakovleva, A. I., Reichart, G.-J., Aleksandrova, G. N., Gnibidenko, Z. N., Schouten, S., and Sluijs, A.: Paleocene–Eocene warming and biotic response in the epicontinental West Siberian Sea, Geology, 42, 767–770, https://doi.org/10.1130/G35724.1, 2014.

Grossman, E. L. and Ku, T.-L.: Oxygen and carbon isotope fractionation in biogenic aragonite: temperature effects, Chem. Geol., 59, 59–74, https://doi.org/10.1016/0168-9622(86)90057-6, 1986.

Hemingway, J. D. and Henkes, G. A.: A disordered kinetic model for clumped isotope bond reordering in carbonates, Earth Planet. Sc. Lett., 566, 116962, https://doi.org/10.1016/j.epsl.2021.116962, 2021.

Henkes, G. A., Passey, B. H., Grossman, E. L., Shenton, B. J., Pérez-Huerta, A., and Yancey, T. E.: Temperature limits for preservation of primary calcite clumped isotope paleotemperatures, Geochim. Cosmochim. Ac., 139, 362–382, https://doi.org/10.1016/j.gca.2014.04.040, 2014.

Huber, M. and Caballero, R.: The early Eocene equable climate problem revisited, Clim. Past, 7, 603–633, https://doi.org/10.5194/cp-7-603-2011, 2011.

Jenkyns, H. C. and Clayton, C. J.: Black shales and carbon isotopes in pelagic sediments from the Tethyan Lower Jurassic, Sedimentology, 33, 87–106, https://doi.org/10.1111/j.1365-3091.1986.tb00746.x, 1986.

Jenkyns, H. C., Schouten-Huibers, L., Schouten, S., and Sinninghe Damsté, J. S.: Warm Middle Jurassic–Early Cretaceous high-latitude sea-surface temperatures from the Southern Ocean, Clim. Past, 8, 215–226, https://doi.org/10.5194/cp-8-215-2012, 2012.

Keating-Bitonti, C. R., Ivany, L. C., Affek, H. P., Douglas, P., and Samson, S. D.: Warm, not super-hot, temperatures in the early Eocene subtropics, Geology, 39, 771–774, https://doi.org/10.1130/G32054.1, 2011.

Kerimov, V. Yu., Shcherbina, Yu. V., and Ivanov, A. A.: Formation conditions and evolution of oil and gas source strata of the Laptev sea shelf ore and gas province, Izvestiya Vysshikh Uchebnykh Zavedeniy. Geologiya i Razvedka, 3, 46–59, https://doi.org/10.32454/0016-7762-2020-63-3-46-59, 2020.

Killam, D. E. and Clapham, M. E.: Identifying the ticks of bivalve shell clocks: seasonal growth in relation to temperature and food supply, PALAIOS, 33, 228–236, https://doi.org/10.2110/palo.2017.072, 2018.

Kim, S.-T. and O'Neil, J. R.: Equilibrium and nonequilibrium oxygen isotope effects in synthetic carbonates, Geochim. Cosmochim. Ac., 61, 3461–3475, https://doi.org/10.1016/S0016-7037(97)00169-5, 1997.

Kim, S.-T., Mucci, A., and Taylor, B. E.: Phosphoric acid fractionation factors for calcite and aragonite between 25 and 75 °C: Revisited, Chem. Geol., 246, 135–146, https://doi.org/10.1016/j.chemgeo.2007.08.005, 2007.

Krencker, F. N., Bodin, S., Hoffmann, R., Suan, G., Mattioli, E., Kabiri, L., Föllmi, K. B., and Immenhauser, A.: The middle Toarcian cold snap: Trigger of mass extinction and carbonate factory demise, Glob. Planet. Change, 15, 64–78, https://doi.org/10.1016/j.gloplacha.2014.03.008, 2014.

Laugié, M., Donnadieu, Y., Ladant, J.-B., Green, J. A. M., Bopp, L., and Raisson, F.: Stripping back the modern to reveal the Cenomanian–Turonian climate and temperature gradient underneath, Clim. Past, 16, 953–971, https://doi.org/10.5194/cp-16-953-2020, 2020.

Li, X., Wang, J., Rasbury, T., Zhou, M., Wei, Z., and Zhang, C.: Early Jurassic climate and atmospheric CO_2 concentration in the Sichuan paleobasin, southwestern China, Clim. Past, 16, 2055–2074, https://doi.org/10.5194/cp-16-2055-2020, 2020.

Lunt, D. J., Dunkley Jones, T., Heinemann, M., Huber, M., LeGrande, A., Winguth, A., Loptson, C., Marotzke, J., Roberts, C. D., Tindall, J., Valdes, P., and Winguth, C.: A model–data comparison for a multi-model ensemble of early Eocene atmosphere–ocean simulations: EoMIP, Clim. Past, 8, 1717–1736, https://doi.org/10.5194/cp-8-1717-2012, 2012.

Markwick, P. J.: Fossil crocodilians as indicators of Late Cretaceous and Cenozoic climates: implications for using palaeontological data in reconstructing palaeoclimate, Palaeogeogr. Palaeocl.,

137, 205–271, https://doi.org/10.1016/S0031-0182(97)00108-9, 1998.

McElwain, J. C., Wade-Murphy, J., and Hesselbo, S. P.: Changes in carbon dioxide during an oceanic anoxic event linked to intrusion into Gondwana coals, Nature, 435, 479–482, https://doi.org/10.1038/nature03618, 2005.

Meyer, K. W., Petersen, S. V., Lohmann, K. C., and Winkelstern, I. Z.: Climate of the Late Cretaceous North American Gulf and Atlantic Coasts, Cretaceous Res., 89, 160–173, https://doi.org/10.1016/j.cretres.2018.03.017, 2018.

Nikitenko, B. L. and Mickey, M. B.: Foraminifera and ostracodes across the Pliensbachian-Toarcian boundary in the Arctic Realm (stratigraphy, palaeobiogeography and biofacies), Geological Society, London, Special Publications, 230, 137–174, https://doi.org/10.1144/GSL.SP.2004.230.01.08, 2004.

Nikitenko, B. L., Shurygin, B. N., Knyazev, V. G., Meledina, S. V., Dzyuba, O. S., Lebedeva, N. K., Peshchevitskaya, E. B., Glinskikh, L. A., Goryacheva, A. A., and Khafaeva, S. N.: Jurassic and Cretaceous stratigraphy of the Anabar area (Arctic Siberia, Laptev Sea coast) and the Boreal zonal standard, Russ. Geol. Geophys.+, 54, 808–837, https://doi.org/10.1016/j.rgg.2013.07.005, 2013.

Nooitgedacht, C. W., van der Lubbe, H. J. L., Ziegler, M., and Staudigel, P. T.: Internal water facilitates thermal resetting of clumped isotopes in biogenic aragonite, Geochem. Geophy. Geosy., 22, e2021GC009730, https://doi.org/10.1029/2021GC009730, 2021.

O'Brien, C. L., Robinson, S. A., Pancost, R. D., Sinninghe Damsté, J. S., Schouten, S., Lunt, D. J., Alsenz, H., Bornemann, A., Bottini, C., Brassell, S. C., Farnsworth, A., Forster, A., Huber, B. T., Inglis, G. N., Jenkyns, H. C., Linnert, C., Littler, K., Markwick, P., McAnena, A., Mutterlose, J., Naafs, B. D. A., Püttmann, W., Sluijs, A., van Helmond, N. A. G. M., Vellekoop, J., Wagner, T., and Wrobel, N. E.: Cretaceous sea-surface temperature evolution: Constraints from TEX_{86} and planktonic foraminiferal oxygen isotopes, Earth-Sci. Rev., 172, 224–247, https://doi.org/10.1016/j.earscirev.2017.07.012, 2017.

O'Connor, L. K., Robinson, S. A., Naafs, B. D. A., Jenkyns, H. C., Henson, S., Clarke, M., and Pancost, R. D.: Late Cretaceous Temperature Evolution of the Southern High Latitudes: A TEX86 Perspective, Paleoceanography and Paleoclimatology, 34, 436–454, https://doi.org/10.1029/2018PA003546, 2019.

Pagani, M., Pedentchouk, N., Huber, M., Sluijs, A., Schouten, S., Brinkhuis, H., Damste, J. S. S., and Dickens, G. R.: Arctic hydrology during global warming at the Palaeocene/Eocene thermal maximum, Nature, 442, 671–675, https://doi.org/10.1038/nature05043, 2006.

Peck, L. S., Colman, J. G., and Murray, A. W. A.: Growth and tissue mass cycles in the infaunal bivalve Yoldia eightsi at Signy Island, Antarctica, Polar Biol., 23, 420–428, https://doi.org/10.1007/s003000050463, 2000.

Petersen, S. V., Dutton, A., and Lohmann, K. C.: End-Cretaceous extinction in Antarctica linked to both Deccan volcanism and meteorite impact via climate change, Nat. Commun., 7, 12079, https://doi.org/10.1038/ncomms12079, 2016a.

Petersen, S. V., Tabor, C. R., Lohmann, K. C., Poulsen, C. J., Meyer, K. W., Carpenter, S. J., Erickson, J. M., Matsunaga, K. K. S., Smith, S. Y., and Sheldon, N. D.: Temperature and salinity of the Late Cretaceous Western Interior Seaway, Geology, 44, 903–906, https://doi.org/10.1130/G38311.1, 2016b.

Pouech, J., Amiot, R., Lécuyer, C., Mazin, J.-M., Martineau, F., and Fourel, F.: Oxygen isotope composition of vertebrate phosphates from Cherves-de-Cognac (Berriasian, France): Environmental and ecological significance, Palaeogeogr. Palaeocl., 410, 290–299, https://doi.org/10.1016/j.palaeo.2014.05.036, 2014.

Price, G. D., Bajnai, D., and Fiebig, J.: Carbonate clumped isotope evidence for latitudinal seawater temperature gradients and the oxygen isotope composition of Early Cretaceous seas, Palaeogeogr. Palaeocl., 552, 109777, https://doi.org/10.1016/j.palaeo.2020.109777, 2020.

Robinson, S. A., Ruhl, M., Astley, D. L., Naafs, B. D. A., Farnsworth, A. J., Bown, P. R., Jenkyns, H. C., Lunt, D. J., O'Brien, C., Pancost, R. D., and Markwick, P. J.: Early Jurassic North Atlantic sea-surface temperatures from TEX_{86} palaeothermometry, Sedimentology, 64, 215–230, https://doi.org/10.1111/sed.12321, 2017.

Roche, D. M., Donnadieu, Y., Pucéat, E., and Paillard, D.: Effect of changes in $\delta^{18}O$ content of the surface ocean on estimated sea surface temperatures in past warm climate, Paleoceanography, 21, PA2023, https://doi.org/10.1029/2005PA001220, 2006.

Rogov, M. A., Zverkov, N. G., Zakharov, V. A., and Arkhangelsky, M. S.: Marine Reptiles and Climates of the Jurassic and Cretaceous of Siberia, Stratigr. Geol. Correl., 27, 398–423, https://doi.org/10.1134/S0869593819040051, 2019.

Rozanski, K., Araguas-Araguas, L., and Gonfiantini, R.: Relation Between Long-Term Trends of Oxygen-18 Isotope Composition of Precipitation and Climate, Science, 258, 981–985, https://doi.org/10.1126/science.258.5084.981, 1992.

Ruebsam, W., Reolid, M., Sabatino, N., Masetti, D., and Schwark, L.: Molecular paleothermometry of the early Toarcian climate perturbation, Glob. Planet. Change, 195, 103351, https://doi.org/10.1016/j.gloplacha.2020.103351, 2020.

Schöne, B. R.: The curse of physiology—challenges and opportunities in the interpretation of geochemical data from mollusk shells, Geo-Mar. Lett., 28, 269–285, https://doi.org/10.1007/s00367-008-0114-6, 2008.

Shackleton, N. J. and Kennett, J. P.: Paleotemperature history of the Cenozoic and the initiation of Antarctic glaciation: oxygen and carbon isotope analyses in DSDP Sites 277,279, and 281, Initial Reports of Deep Sea Drilling, 29, 743–756, 1975.

Sluijs, A., Schouten, S., Pagani, M., Woltering, M., Brinkhuis, H., Damsté, J. S. S., Dickens, G. R., Huber, M., Reichart, G.-J., Stein, R., Matthiessen, J., Lourens, L. J., Pedentchouk, N., Backman, J., Moran, K., and the Expedition 302 Scientists: Subtropical Arctic Ocean temperatures during the Palaeocene/Eocene thermal maximum, Nature, 441, 610–613, https://doi.org/10.1038/nature04668, 2006.

Sluijs, A., Frieling, J., Inglis, G. N., Nierop, K. G. J., Peterse, F., Sangiorgi, F., and Schouten, S.: Late Paleocene–early Eocene Arctic Ocean sea surface temperatures: reassessing biomarker paleothermometry at Lomonosov Ridge, Clim. Past, 16, 2381–2400, https://doi.org/10.5194/cp-16-2381-2020, 2020.

Stolper, D. A. and Eiler, J. M.: The kinetics of solid-state isotope-exchange reactions for clumped isotopes: A study of inorganic calcites and apatites from natural and experimental samples, Am. J. Sci., 315, 363–411, https://doi.org/10.2475/05.2015.01, 2015.

Suan, G., Mattioli, E., Pittet, B., Lécuyer, C., Suchéras-Marx, B., Duarte, L. V., Philippe, M., Reggiani, L., and Martineau, F.: Secular environmental precursors to Early Toarcian (Jurassic) extreme climate changes, Earth Planet. Sc. Lett., 290, 448–458, https://doi.org/10.1016/j.epsl.2009.12.047, 2010.

Suan, G., Nikitenko, B. L., Rogov, M. A., Baudin, F., Spangenberg, J. E., Knyazev, V. G., Glinskikh, L. A., Goryacheva, A. A., Adatte, T., Riding, J. B., Föllmi, K. B., Pittet, B., Mattioli, E., and Lécuyer, C.: Polar record of Early Jurassic massive carbon injection, Earth Planet. Sc. Lett., 312, 102–113, https://doi.org/10.1016/j.epsl.2011.09.050, 2011.

Suan, G., Popescu, S.-M., Suc, J.-P., Schnyder, J., Fauquette, S., Baudin, F., Yoon, D., Piepjohn, K., Sobolev, N. N., and Labrousse, L.: Subtropical climate conditions and mangrove growth in Arctic Siberia during the early Eocene, Geology, 45, 539–542, https://doi.org/10.1130/G38547.1, 2017.

Thierry, J.: Middle Toarcian map. 8, in: Altlas Peri-Tethys Palaeogeographical Maps, edited by: Dercourt, J., Gaetani, M., Vrielynck, B., Barrier, E., Biju-Duval, B., Brunet, M. F., Cadet, J. P, Crasquin, S., and Sandulescu, M., CCGM/CGMW, Paris, 61–70, 2000.

Thuy, B., Gale, A. S., and Reich, M.: A new echinoderm Lagerstätte from the Pliensbachian (Early Jurassic) of the French Ardennes, Swiss J. Palaeontol., 130, 173–185, https://doi.org/10.1007/s13358-010-0015-y, 2011.

Tindall, J., Flecker, R., Valdes, P., Schmidt, D. N., Markwick, P., and Harris, J.: Modelling the oxygen isotope distribution of ancient seawater using a coupled ocean–atmosphere GCM: Implications for reconstructing early Eocene climate, Earth Planet. Sc. Lett., 292, 265–273, https://doi.org/10.1016/j.epsl.2009.12.049, 2010.

Torsvik, T. H., Van der Voo, R., Preeden, U., Mac Niocaill, C., Steinberger, B., Doubrovine, P. V., van Hinsbergen, D. J. J., Domeier, M., Gaina, C., Tohver, E., Meert, J. G., McCausland, P. J. A., and Cocks, L. R. M.: Phanerozoic polar wander, palaeogeography and dynamics, Earth-Sci. Rev., 114, 325–368, https://doi.org/10.1016/j.earscirev.2012.06.007, 2012.

Ullmann, C. V., Boyle, R., Duarte, L. V., Hesselbo, S. P., Kasemann, S. A., Klein, T., Lenton, T. M., Piazza, V., and Aberhan, M.: Warm afterglow from the Toarcian Oceanic Anoxic Event drives the success of deep-adapted brachiopods, Sci. Rep.-UK, 10, 6549, https://doi.org/10.1038/s41598-020-63487-6, 2020.

van Baal, R. R., Janssen, R., van der Lubbe, H. J. L., Schulp, A. S., Jagt, J. W. M., and Vonhof, H. B.: Oxygen and carbon stable isotope records of marine vertebrates from the type Maastrichtian, The Netherlands and northeast Belgium (Late Cretaceous), Palaeogeogr. Palaeocl., 392, 71–78, https://doi.org/10.1016/j.palaeo.2013.08.020, 2013.

van Dijk, J., Fernandez, A., Bernasconi, S. M., Caves Rugenstein, J. K., Passey, S. R., and White, T.: Spatial pattern of supergreenhouse warmth controlled by elevated specific humidity, Nat. Geosci., 13, 739–744, https://doi.org/10.1038/s41561-020-00648-2, 2020.

van Hinsbergen, D. J. J., de Groot, L. V., van Schaik, S. J., Spakman, W., Bijl, P. K., Sluijs, A., Langereis, C. G., and Brinkhuis, H.: A Paleolatitude Calculator for Paleoclimate Studies, PLoS ONE, 10, e0126946, https://doi.org/10.1371/journal.pone.0126946, 2015.

Vickers, M. L., Bajnai, D., Price, G. D., Linckens, J., and Fiebig, J.: Southern high-latitude warmth during the Jurassic–Cretaceous: New evidence from clumped isotope thermometry, Geology, 47, 724–728, https://doi.org/10.1130/G46263.1, 2019.

Vickers, M. L., Fernandez, A., Hesselbo, S. P., Price, G. D., Bernasconi, S. M., Lode, S., Ullmann, C. V., Thibault, N., Hougaard, I. W., and Korte, C.: Unravelling Middle to Late Jurassic palaeoceanographic and palaeoclimatic signals in the Hebrides Basin using belemnite clumped isotope thermometry, Earth Planet. Sc. Lett., 546, 116401, https://doi.org/10.1016/j.epsl.2020.116401, 2020.

Vickers, M. L., Bernasconi, S. M., Ullmann, C. V., Lode, S., Looser, N., Morales, L. G., Price, G. D., Wilby, P. R., Hougård, I. W., Hesselbo, S. P., and Korte, C.: Marine temperatures underestimated for past greenhouse climate, Sci. Rep.-UK, 11, 19109, https://doi.org/10.1038/s41598-021-98528-1, 2021.

Vihtakari, M., Renaud, P. E., Clarke, L. J., Whitehouse, M. J., Hop, H., Carroll, M. L., and Ambrose, W. G.: Decoding the oxygen isotope signal for seasonal growth patterns in Arctic bivalves, Palaeogeogr. Palaeocl., 446, 263–283, https://doi.org/10.1016/j.palaeo.2016.01.008, 2016.

Waterlot, G., Bonte, A., and Destombes, J.-P.: Carte géologique de la France à 1 : 50 000, [68], Renwez, France, 1960.

Wierzbowski, H., Bajnai, D., Wacker, U., Rogov, M. A., Fiebig, J., and Tesakova, E. M.: Clumped isotope record of salinity variations in the Subboreal Province at the Middle–Late Jurassic transition, Glob. Planet. Change, 167, 172–189, https://doi.org/10.1016/j.gloplacha.2018.05.014, 2018.

Zakharov, V. A. and Shurygin, B. N.: Biogeography, facies and stratigraphy of the Middle Jurassic of Soviet Arctic (by bivalve molluscs), Transactions of the Institute of Geology and Geophysics, Siberian Branch of the Academy of Science of USSR, 352, 1–206, 1978.

Zardus, J. D.: Protobranch bivalves, Ad. Mar. Biol., 42, 1–65, https://doi.org/10.1016/S0065-2881(02)42012-3, 2002.

Zhou, J., Poulsen, C. J., Pollard, D., and White, T. S.: Simulation of modern and middle Cretaceous marine $\delta^{18}O$ with an ocean-atmosphere general circulation model: Modern, mid-Cretaceous seawater $\delta^{18}O$, Paleoceanography, 23, PA3223, https://doi.org/10.1029/2008PA001596, 2008.

Zhu, J., Poulsen, C. J., Otto-Bliesner, B. L., Liu, Z., Brady, E. C., and Noone, D. C.: Simulation of early Eocene water isotopes using an Earth system model and its implication for past climate reconstruction, Earth Planet. Sc. Lett., 537, 116164, https://doi.org/10.1016/j.epsl.2020.116164, 2020.